Robust graphene-based monoliths of homogeneous ultramicroporosity

by

Teresa J. Bandosz[1, 2*], Shuwen Wang[1] , Daiki Minami[1] and Katsumi Kaneko[1]

[1]Shinshu University

Center for Energy and Environmental Science, 4-17-1 Wakasato, Nagano, 380-8553 Japan

[2]Permamet address: Department of Chemistry, The City College of New York, New York, NY 10031

[*] Whom the correspondence should, be addressed to. Tel.: (212)650-6017; Fax: (212) 650-6107; Email: tbandosz@ccny.cuny.edu

ABSTRACT

Graphite oxide (GO) and graphene monoliths were prepared using the unidirectional freezing of GO water suspension. These materials were saturated with a poly(4 ammonium styrene sulfonic acid) water soluble polymer and then carbonized at 1123 K. This process increases significantly the materials strength and density. A uniform deposition of the polymer-derived carbon on the external layers of the graphene sheets of the monolith was found. The carbon from polymer not only provided more contact between the graphene sheets but apparently increased the overall graphitization level (based on Raman spectra). The modification decreased the electrical resistance by one order of magnitude compared to that of the graphene monolith. N_2 adsorption at 77 K showed that the thus-treated graphene monoliths has quite homogenous pores with the pore width of 0.7 nm. These pores combined with large transport pores and conductive properties make the monoliths tested the promising materials for separation, energy storage and/or gas sensing. The tunability of the properties and pore structure of the robust graphene untramicroporous monolith through the control of chemistry of the initial GO monolith was shown.

Key words

Graphene-based monoliths; electrical resistance; porosity; surface characterization

1. Introduction

Carbon monoliths of specific performance have been actively studied for various applications including separation [1] and gas storage [2], because the monolith form has intriguing advantages such as high electrical and thermal conductivities, high density storage, no intergranular barriers, and easy handling. For these applications the sizes of the pores and their

volumes are of paramount importance. Carbon monoliths are usually obtained using either binders [1] or in binder free process [2,3]. The latter one involves the extrusion method used for organic polymers. Applying binders reduces the performance of an active carbon phase per unit volume and might result in some instability of a monolith for longer applications. Another method is based on template carbonization and an example is a recently reported monolith obtained using porous concrete [5]. Nevertheless, in this approach a post-carbonization additional activation need to be applied to develop the microporosity. Another method is based on soft templates and usually the triblock copolymers (F127) are used as templates [6-8]. Recently developed approach is based on unidirectional freeze drying method for aqueous colloidal system without any binders and it was applied to develop monoliths from polymers [9] or graphite oxides [10,11]. Freeze –thaw cycles have been also proposed as a method of graphite oxide exfoliation [12].

Although the development of porosity in monoliths is essentially important, the methods proposed lead to materials that are not superior to activated carbons in this aspect [3-8]. Of course the shape and mechanical stability of a monolith is essential for industrial applications where powdered activated carbon are rather not desired. This causes that the efforts on the development of monoliths of interesting properties continue.

An advance in the graphene science has directed the attention of the scientist interested in monolith developments to this family of materials. Monoliths based on graphene can find new cutting edge-applications owing to the high electrical and thermal conductivity of graphene layers. Examples are energy storage devices and thermal isolators. Recently an ice-templating derived graphene based monolith of superporosity of 2200 m^2/g and high electrical conductivity has been described by Kaneko and coworkers [11]. Unfortunately, even though the dispersive

forces between binder free “self assembled” graphene sheets are strong enough to provide a predetermined shape the structure is rather weak.

We have several approaches for developing the graphene based monoliths having the specific properties of graphenes. The objective of this paper is to develop a new type of graphene-based monolith with very homogenous porosity in the range of ultramicropores being promising for separation technology. In their structure the integrity of the graphene layers is preserved providing the conductive properties. They are obtained using an environmentally friendly method by saturation of the graphite oxide monolith with water-soluble commodity polymer followed by its carbonization. This simple treatment has provided a novel graphene-based monolith of quite uniform nanoporosity in addition to the mechanical strength.

2. Experimental

2.1. Monolith coating procedure

GO monoliths were obtained from 1:1 mixture of GO obtained from Bay carbon graphite (Michigan, USA) and Madagascar graphite (obtained using Hummers method [11]). The details on the preparation of GO are described elsewhere [10]. Dense suspensions/pastes of GO were frozen with liquid nitrogen and freeze dried for three days. The brownish GO monolith obtained in this process is referred to as MGO. A subsample of MGO was partially reduced into the graphene monolith by treatment in argon at 623 K with heating rate 1.4 deg/min and holding time 30 min. This sample is referred to as MR. Both MGO and MR were soaked in 15 wt % aqueous solution of 4-ammonium styrene sulfonic acid (ASSA) polymer for four hours. MR with the polymer was then dried in room temperature for three days (denoted as MRP) and MGO with the polymer was freeze-dried for three days (denoted as MGOP). Then the MGOP sample was reduced at 623 K at the same conditions as the initial GO and it is referred to as MPR. All three

samples, MRP, MPR along with MR were heated at 1123 K in argon with a heating rate 30 deg/min and soaking time 1 hour. The final samples are referred to HT-MRP, HT-MPR and HT-MR following the treatment procedures.

For elucidate clearly the role of the carbon phase the ASSA polymer was carbonized in argon in two steps at 623 K (heating rate 1.4 deg/min) with holding time 30 min and then at 1123 K in argon with the heating rate 30 deg/min and holding time 30 min. The sample is referred to as PC.

2. 2. Characterization

2.2.1. Determination of apparent density

The estimation of the monolith density was performed by measurement of their sizes (diameter and length) and weights.

2.2.2.Electrical resistance

Electrical resistance was measured on the external surface of monoliths using a four point probe method (Leresta-GP MCP-T610; Mitsubishi). The resistivity was measured along the monolith length (L) and on the cross section (D) surfaces.

2.2.3. *Optical microscope*

The optical microscope images were obtained on Olympus DP73 in a bright mode with the low magnification of 5k owing to the high degree of surface roughness.

2.2.4 FTIR

FTIR measurement was carried out using a Nicolet 6700 spectrometer using the attenuated total reflectance (ATR) method with a diamond crystal for the powdered samples without KBr addition. The spectrum was generated and collected 32 times and corrected for the background noise..

2.2.5. TA/MS analysis

Thermogravimetric (TG) curves were obtained using a Rigaku TG-DTA-PIMS 410/S, equipped with a mass spectrometer. The GOM and composite samples were heated up to 1123 K (10 deg min^{-1}) under a helium flow (300 mL min^{-1}). The composition of released gases was evaluated by MS and m/z evolution profiles as a function of temperature were obtained.

2.2.6. Raman spectroscopy

The Raman spectra were obtained on a Renishaw InVia Raman spectrometer fitted with microscope and a 5 × objective using a 532 nm laser with 1% power and exposure time 10 s.

2.2.7. SEM and TEM

SEM images were collected on JEOL JSM 700F/IV field scanning emission electron microscope and JEOL-JSM-6335FS with 20 kV and 10 kV voltage applied, respectively. High resolution TEM images were collected on a high resolution transimission electron microscope (JEM-40000 FX, JEO).

2.2.8. Evaluation of porosity

Nitrogen adsorption isotherms were measured at 77 K on ASAP2020 (Micromeritics). Samples were out-gassed at 393 K for two hours. The surface areas and the volumes pores were determined The former was obtained using the BET and SPE methods [13]. The pore volume along with the pore size distributions were obtained using Density Functional Theory approach (www.NLDFT.com) [14].

2.2.9. Testing of mechanical strength

The evaluation of mechanical strength was done by weights of 20 g, 50 g and 100g on the initial and modified monoliths.

3. Results and Discussion

3.1. Morphological and mechanical properties of the monoliths.

The pictures of the obtained monoliths are presented in Figure 1. As seen as a result of the treatment applied the color and the geometrical dimensions of the monoliths changed. A slight shrinkage was observed. More importantly, the samples treated with the polymer became much harder than HT-MR. The initial MGO is a very soft and easy to disintegrate material. It was hypothesized that dispersive forces are responsible for the arrangement of GO particles during the rapid freezing and slow drying process [10]. Its texture resembles that of the paper filters with extended graphene oxide flakes arranged with the axial length of the monolith (freezing direction). Reduction at 623 K makes the structure slightly more stable, but it still remains very "fabric-soft". During this process a slow decomposition of epoxy groups present on the basal planes [15] results in an increase of dispersive interactions between the distorted graphene sheets. These interactions are even more enforced when the GO is reduced at 1123 K. Nevertheless, the soft texture of the monolith remains after that high temperature treatment. Saturation of GO with the polymer, followed by drying, results in a visible shrinkage of the monoliths (about 30 volume %).

The samples were exposed to various external weights to quantify the differences in the mechanical strength of MGO and HT-MR, and the polymer enforced monolith (Figure 2). The MGO and HT-MR could be tested only when the force was applied horizontally to the monolith length since the disintegration was observed with any attempts to place monoliths in a free-stand position. For GOM and HT-MR visible dents/recesses are seen directly under a weight when 20 g and 50 g weights were applied, respectively. On the other hand, HT-MRP shows a remarkable strength and no changes were noticed even when 100 g was applied in both vertical and

horizontal directions of the monolith. The tolerable maximum pressure indicates that the sample can maintain the external pressure of at least 30 kPa without any visible sign of a structural disintegration.

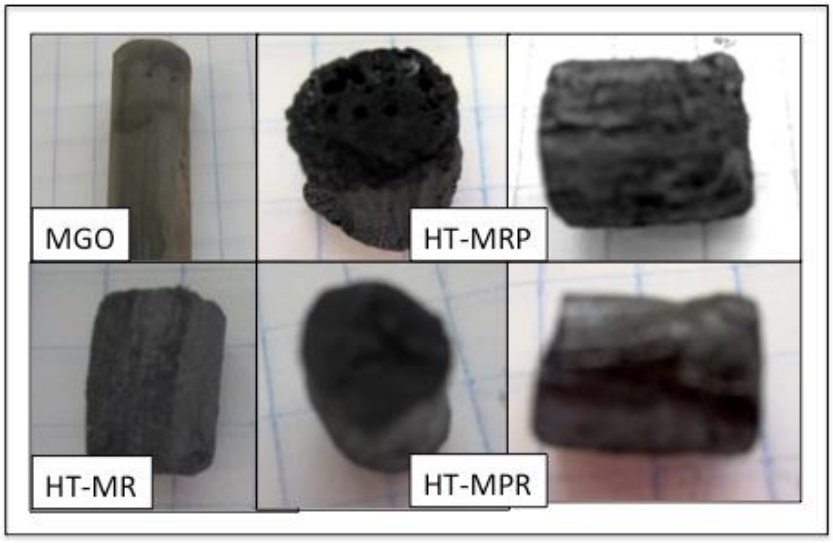

Figure 1. Appearance of the monoliths, initial and after the final modifications. One grid on the background paper is 5 x 5 mm.

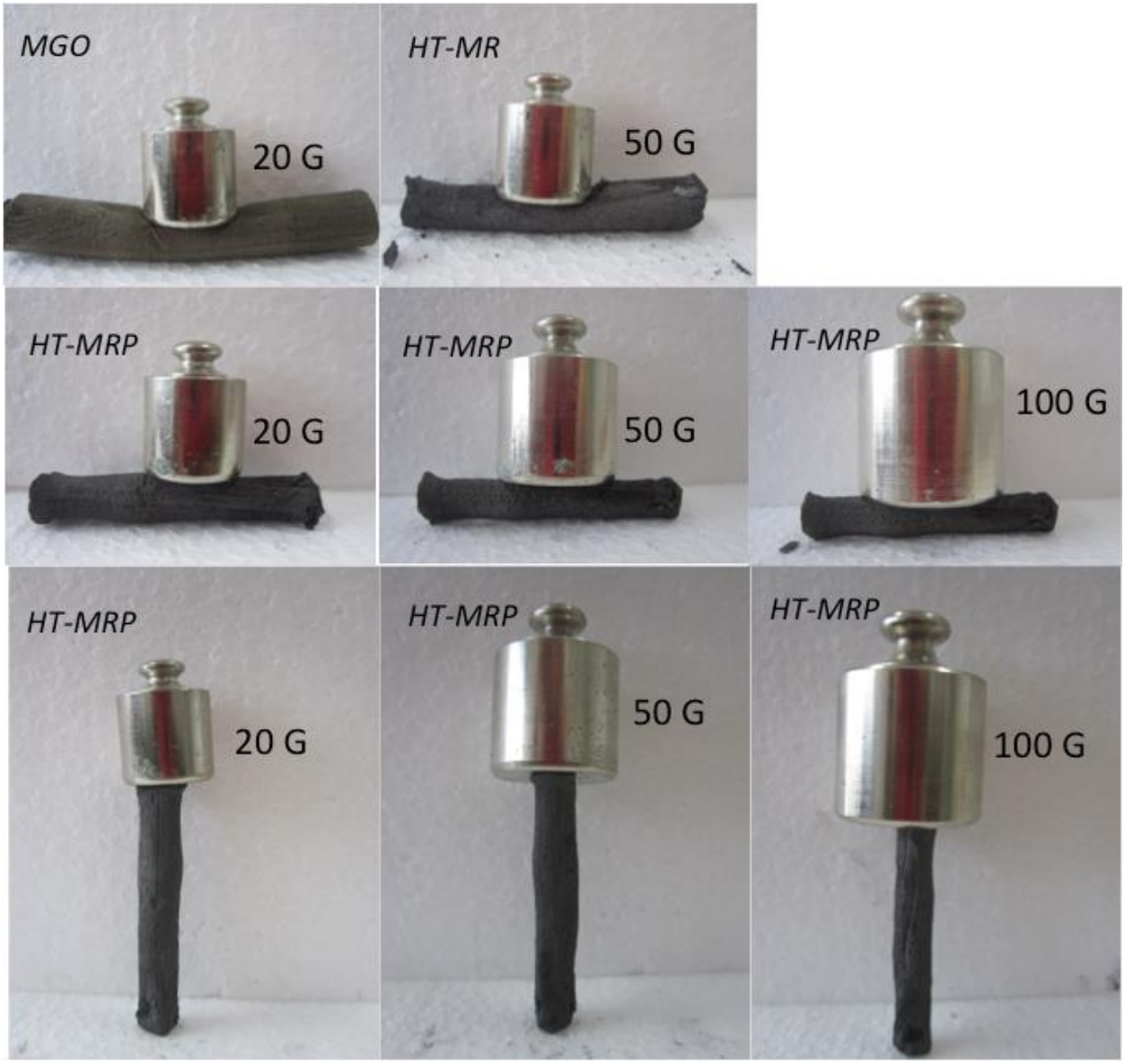

Figure 2. Comparison of the strength of the initial and modified monoliths. The diameter of HT-MRP monolith is 7 mm.

The MGO sample gains about 3.5 times of its original weight as a result of the polymer saturation and freeze-drying. The last process visibly removed some polymer solution from the monolith volume. The reduced monolith MR adsorbed even more polymer (12 times of its

original mass). It is likely owing to air drying and to that fact that reduction removed epoxy groups resulting in a more hydrophobic nature of graphene sheet and thus in a more favorable environment for adsorption of aromatic rings of the polymer via π–π interactions. The detailed analysis of the changes in the sample weight at different steps of the preparation is presented in Supplementary Information.

3.2.Nanoscopic morphology

Optical images of the external surfaces of the HT-MR, HT-MPR and HT-MRP are presented in Figure 1S of Supplementary Information. The composites visibly exhibit a denser arrangement of carbons grains caused by the deposition of the polymer-derived carbon phase. A further insight into the texture is provided by SEM images collected in Figures 3 and 4. The surfaces of MGO and HT-MR consist of loosely connected, twisted and wrinkled flakes of GO of about 20 μm in diameter and 10 nm thick (Figure 3). Those loose connections, even though they provide enough strength to maintain the integrity of the composites, must affect negatively the electronic conductivity of the monolith. Addition of the polymer totally changes the texture. In Figure 4 the surface of MPR is presented where the polymer is visible in the thermally changed but still not in the fully carbonized form. Here the flake of GO embedded in the polymer is clearly seen. The arrangement suggests that the polymer exhibits a very high adhesion to GO and the thickness of its layer is almost equal on the both sides of the graphene flake (about 500 nm). The charred polymer texture follows a wrinkled surface of the GO flakes.

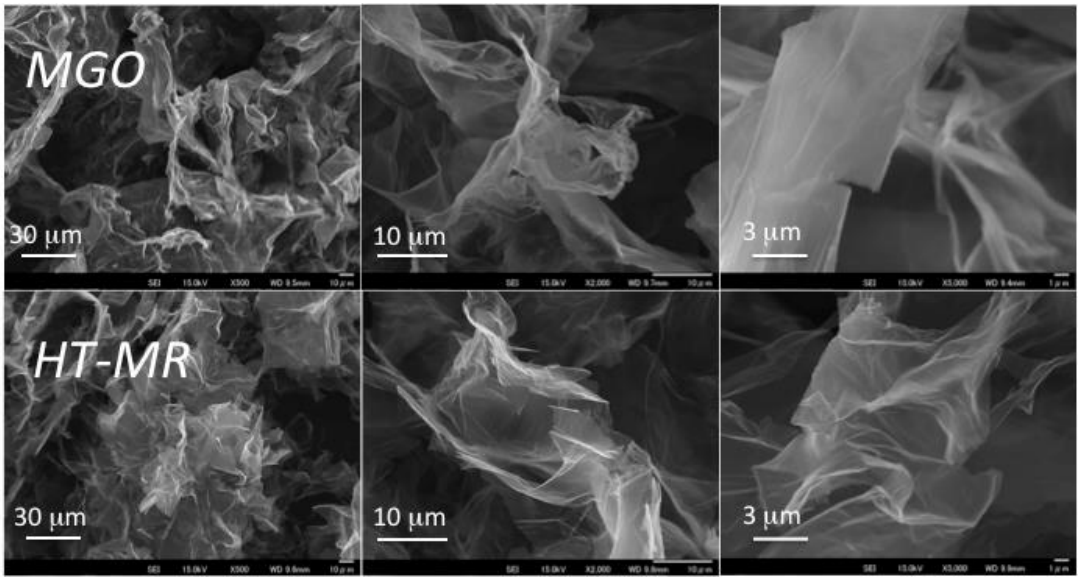

Figure 3. SEM images for MGO and HT-MR.

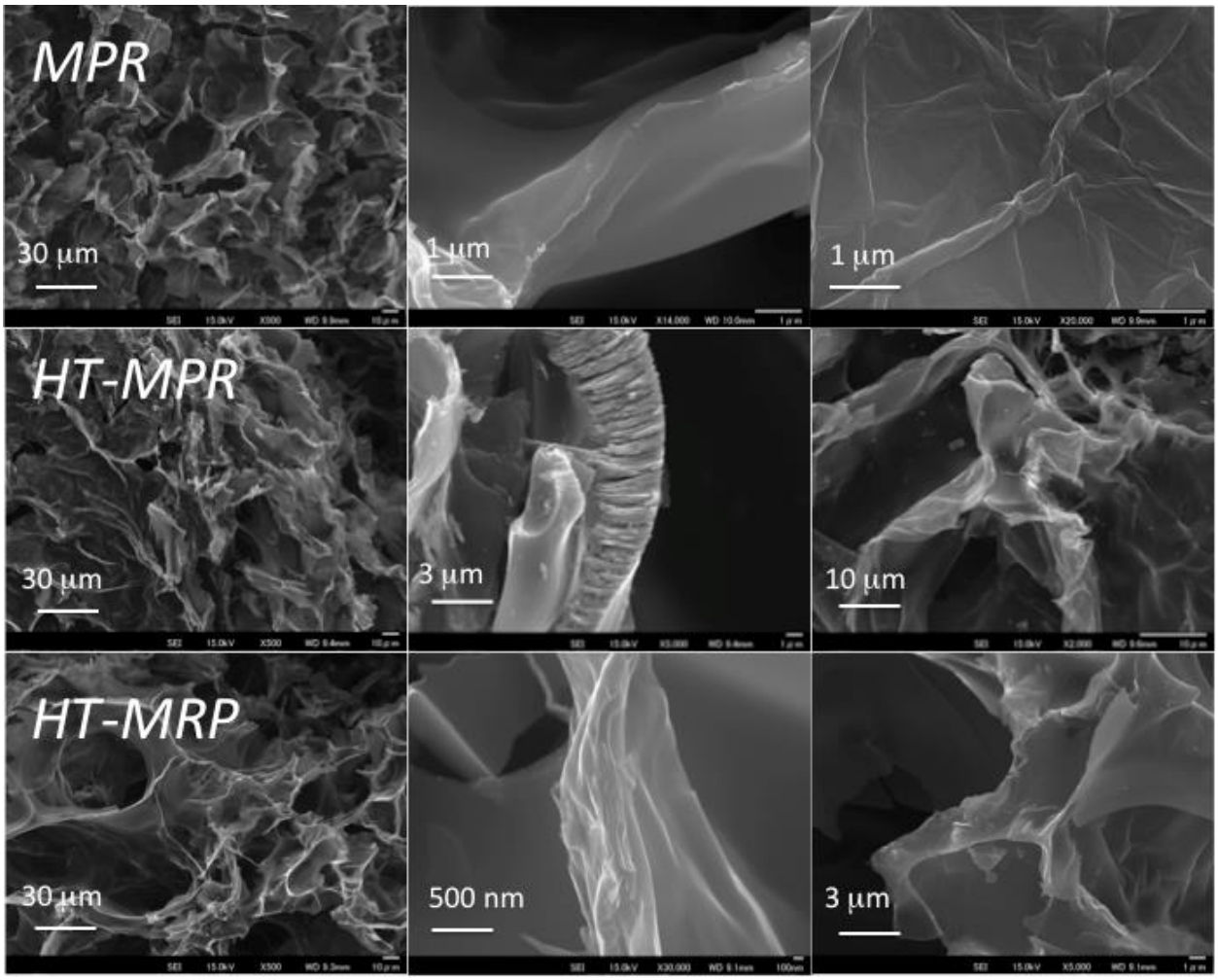

Figure 4. SEM images for the polymer treated monoliths,

There are visible differences in the texture of HT-MRP and HT-MPR with the latter sample exhibiting a denser texture with smaller particles. The thickness of polymer-derived carbon "walls" in the case of HT-MRP is about 200 nm. In the case of HT-MPR the polymer-originated phase seems to be more bulky even reaching 2 μm in its thickness with visible cracks in the amorphous carbon phase. This might be the result of the reaction of the polymer with the GO surface and formation of a specific resin that is more thermally stable than is the polymer itself.

HRTEM images for the reinforced monoliths are presented in Figure 5. The images of HT-MRP show the presence of intact graphene layers, graphene covered with the carbon and the amorphous carbons phase. On the other hand, for HT-MPR the unmodified graphene layers cannot be detected, which supports the formation of a resin on their surface as a result of the reactions of GO functional groups with the sulfonic groups of the polymer. This resin is converted into the amorphous carbon phase during the carbonization process and it covers the GO sheets.

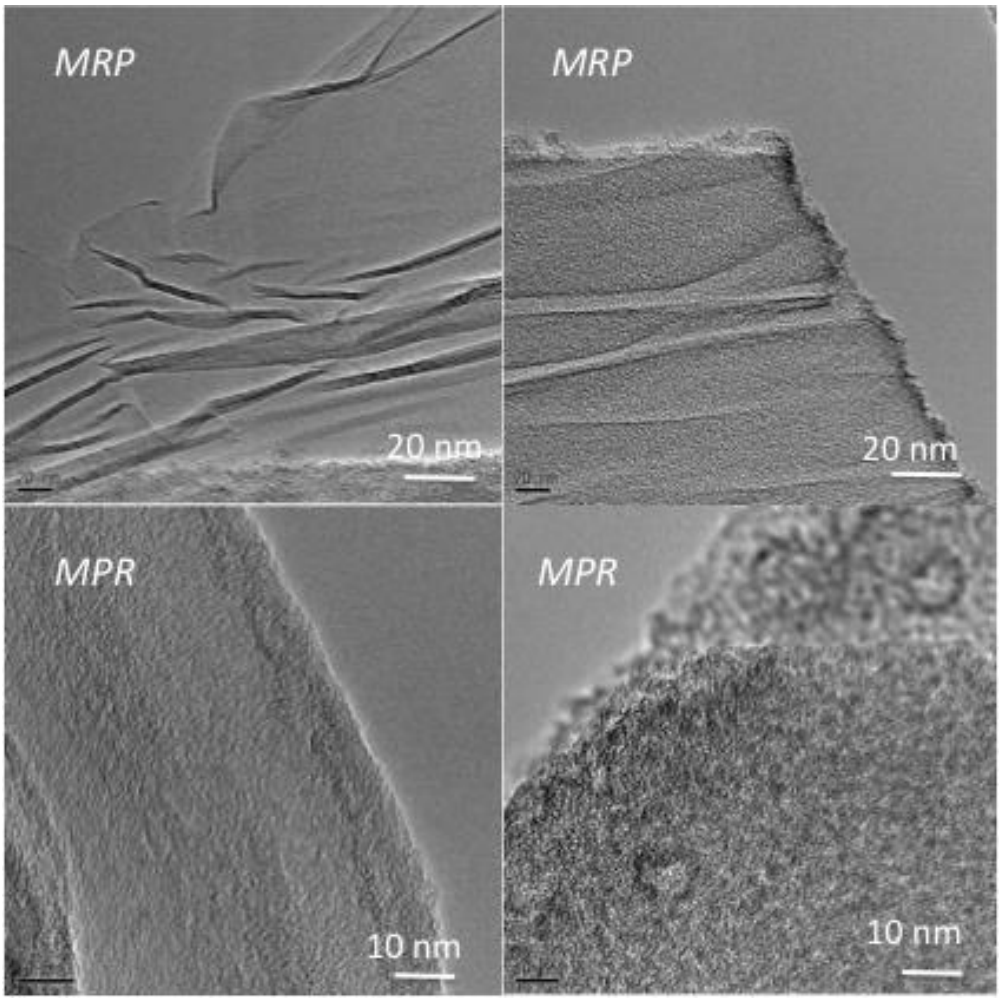

Figure 5. HRTEM images of the monolith texture.

3.3. Changes in chemical and physical properties on coating.

Although the experimental procedure is very simple, the polymer embedded in GO gives a sophisticated alteration of the monolith structure. During the saturation with the polymer especially in the case of the MGO sample, the reactions of sulfonic groups of the polymer with epoxy groups of the GO in the acidic environment can take place resulting in the formation of sulfonic acid ester bound to the graphene sheet surface [16, 17]. A detailed analysis of the changes in the weight of the monolith during its preparation is provided in Supplementary Information. The results suggest that a significant amount of the partially charred polymer bound to the surface and thus thermally stable is still present within the structure of the MPR sample. This phase apparently follows different carbonization pattern than that exhibited by ASSA (Figure 2S of SI).

Heating the polymer-treated samples at 1123 K resulted in the monoliths of considerable physical strength though brittle when cut. The results indicate that even though the high temperature reduction was applied to MR, the monolith still contains a significant amount of oxygen groups, likely OH, which are expected to decompose at high temperatures [18]. Interestingly, the extent of the weight loss for the polymer-treated monolith is not in an agreement with the difference in the content of the polymer, which was adsorbed in greater quantity by MR than by the MGO sample (Supplementary Information). Apparently the initial reaction of the polymer with GO and the heat treatment at 623 K give rise to the composite material which decomposes at higher temperatures than that obtained by a direct carbonization of the polymer adsorbed on the reduced MR monolith. In fact, more of the charred polymer phase was present on MPR treated at 623 K than that on MRP treated at the same conditions.

Table 1. Electrical resistance, apparent density ρ and the ratios of the D/G band intensity from the Raman spectra

Sample	R-L [Ω]	R-D [Ω]	ρ□ □g/cm^3]	I_D/I_G
MGO	1.7 x 10^7	4.0 x 10^6	0.042	0.84
MR	50	90	0.016	1.06
HT-MR	14	13	0.015	1.09
HT-MRP	5.5	4.4	0.091	1.00
HT-MPR	1.2	1.6	0.169	1.07
PC	5.5*	NA	NA	---

*resistance measured on the solid piece of the carbonized polymer of about 4 cm^2

The evaluation of materials' density was carried out based on the estimated geometrical sizes of the samples and their weight. The results are collected in Table 1. Significant differences are seen. MGO is a very light material with the density of 0.042 g/cm^3. Obviously there is a large volume of void spaces between the aligned GO paper/fabric-like sheets. Reduction at 623 K decreases the density almost three times as a result of the removal of a significant amount of oxygen. Then further heating decreases the density only slightly (~ 10 %). Addition of the polymer-based phase to both MGO and MR visibly increases the density of the monoliths, which apparently increases their strength and mechanical resistance. The densest material is obtained when the MGO initial monolith is treated with the polymer. It happens in spite of the fact that the amount of the polymer gained by the sample was much greater for the MR monolith. Apparently hypothesized above reaction of the monolith surface with the polymer reflected in changes in the thermal decomposition pattern that led to the denser product. Another reason for these differences might be in the kinetics of the polymer decomposition and the effects of the released gases on the porosity development in the polymer based carbon. Thus in the case of HT-MRP,

the fast released gases from the decomposition of the polymer could expand the GO layers resulting in large voids seen in the outer surface of the monolith (Figure 1). On the other hand, during the slow heating to 623 K of the polymer present in MGOP the release of gases was much less rapid. This process was stopped and the partially charred polymer was stabilized at 623 K before undergoing a fast pyrolysis to 1123 K. Thermal analysis and the changes in the polymer chemistry during heating clearly show a significant mass loss at about 623 K (Figure 2S). This effect can be related to the decomposition of sulfonic acid and removal of ammonia (see the polymer chemical formula in Figure 3S of Supplementary Information). Then at about 773 K aromatization of the rings should take place with the removal of hydrocarbons [19]. The fast removal/decomposition of sulfonic groups and ammonia might affect in a negative way the development of porosity, if the polymer is present on the surface of the monolith in an unchanged form. On the other hand, the decomposition of epoxy groups during heating at 623 K in the presence of the decomposing polymer on the surface should contribute to the porosity development in the char/carbon phase. This is not expected be the case for the HT-MRP sample.

Table 1 shows that the reduction of the GO monolith at 623 K significantly increased the electrical conductivity of five orders of magnitude as a result of the removal of oxygen groups [15]. Then the resistance further decreased of one order of magnitude after carbonization at 1123 K. The carbon coating caused an order of magnitude improvement in the monolith conductivity. It is reported that the carbon from the same polymer had a high electrical conductivity due to the unique structure consisting of 10 nm graphitic domains [20]. The obtained highly electrical conductive properties are very important for an application of these monoliths for energy storage [21] or as catalysts for oxygen reduction [22] or water splitting processes where the fast electron transfer is a desired feature [23]. Interestingly, the resistance values measured are comparable

through both dimensions, especially for the monoliths heated at 1123K indicating the presence of conductive paths in various directions of the monoliths' volumes.

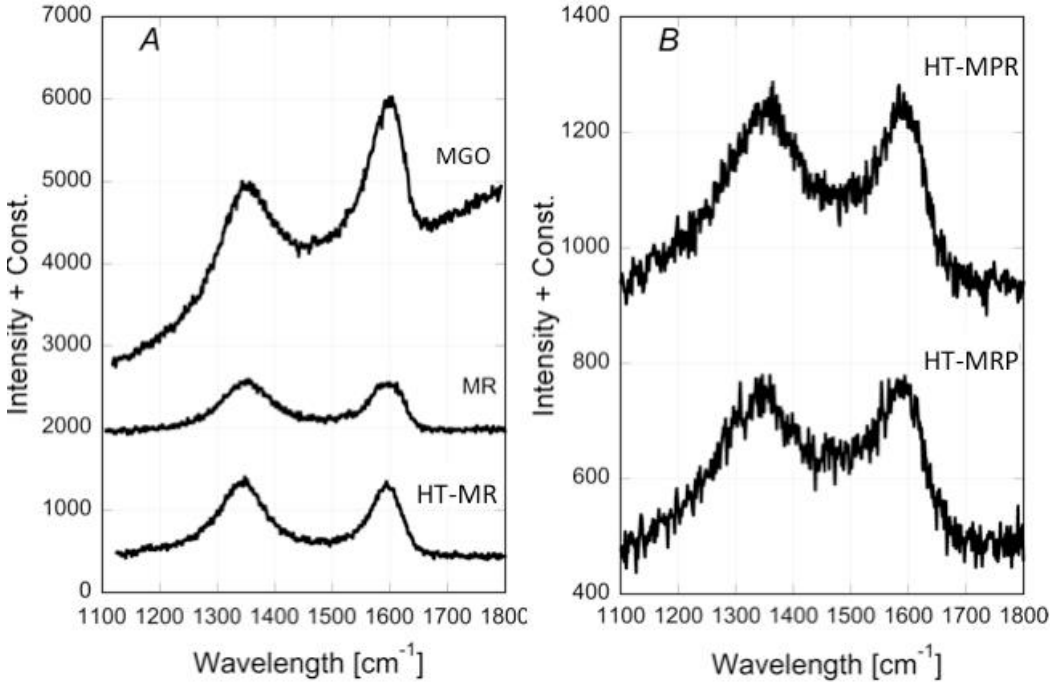

Figure 6. Raman spectra for the series of the graphene-based (A) and carbon-reinforced monoliths (B).

Raman spectra are collected in Figure 6. A distinct pair of absorption bands around 1350 cm^{-1} (D band) and 1580 cm^{-1} (G band) is visible for all samples. The G band and D band are assigned to the hexagonal carbon plane and crystal defects or imperfections in these planes, respectively [24]. Moreover, the ratio of the relative intensity of these two bands (I_D/I_G) (Table 2) is considered as a measure of the number of defects in the carbonaceous materials [24]. The lower ratio indicates the higher graphitization level. Interestingly, the thermal treatment of the monolith gradually increased the defects in the monolith, which was caused by the removal of oxygen groups. The electrical resistivity is much more sensitive to the oxygen removal than the defectiveness of the

carbon frame observed by Raman spectroscopy. The carbon coating decreases the I_D/I_G ratio compared to that for HT-MR. This is an indication that the carbon phase increases the overall level of graphitization in these materials. This trend is also consistent with an increase in the monolith electrical conductivity.

3.5 Mechanism of the carbon reinforcement of the monoliths

The FTIR spectra for the graphene monoliths are presented in Figure 4S of Supplementary Information along with the detailed assignment of absorption bands. While for the MGO the typical bands representing oxygen groups are visible [25], after the treatment at 1123 K only residual oxygen bonded to carbon is seen on the spectra for all samples. These results indicate that even though the polymer has been introduced to the monolith and carbonized, it does not change the infrared absorption spectrum of the graphene based matrix. Moreover, the presence of sulfur, oxygen and nitrogen in the polymer, does not give the apparent absorption bands inherent to their surface functional groups. The thermal treatment likely removed the majority of heteroatoms from the carbon phase. The reason for that significant reduction can be also in a reducing effect of the graphene phase itself. On the other hand, the spectrum for the polymer-derived carbon PC shows multiple peaks coming from the abundance of oxygen groups, which suggests the low level of aromatization/carbonization [25].

The thermal analysis results for the graphene based monoliths and polymer-enforced counterparts are collected in Figures 6S of Supplementary Information. They confirm the reduced nature of the graphene-based monolith as a result of high temperature treatment and the decomposition of surface oxygen groups [17]. The m/z thermal profiles for MR and HT-MR show the similarities in the removal pattern of surface decomposition products (Figure 5S and 6S

of Supplementary Information), although the intensities of the current for the latter sample are at least three orders of magnitude smaller than for the former one.

Thermal analysis data for the polymer treated monoliths show slight differences in materials thermal stability/surface chemistry (Figure 7 B). Both samples are very stable and lose only up to 3.5 % mass loss and HT-MPR is slightly less reactive with the atmospheric oxygen than the sample obtained from the reduced monolith saturated with the polymer, HT-MRP. It is plausible to assume that the surface chemistry of the monolith has an important effect on the properties of the carbon phase and the surface bounded phase, which might form on the surface of the MGO sample. It apparently leads to the more stable carbon phase than that in the case of the reduced GO -based monolith.

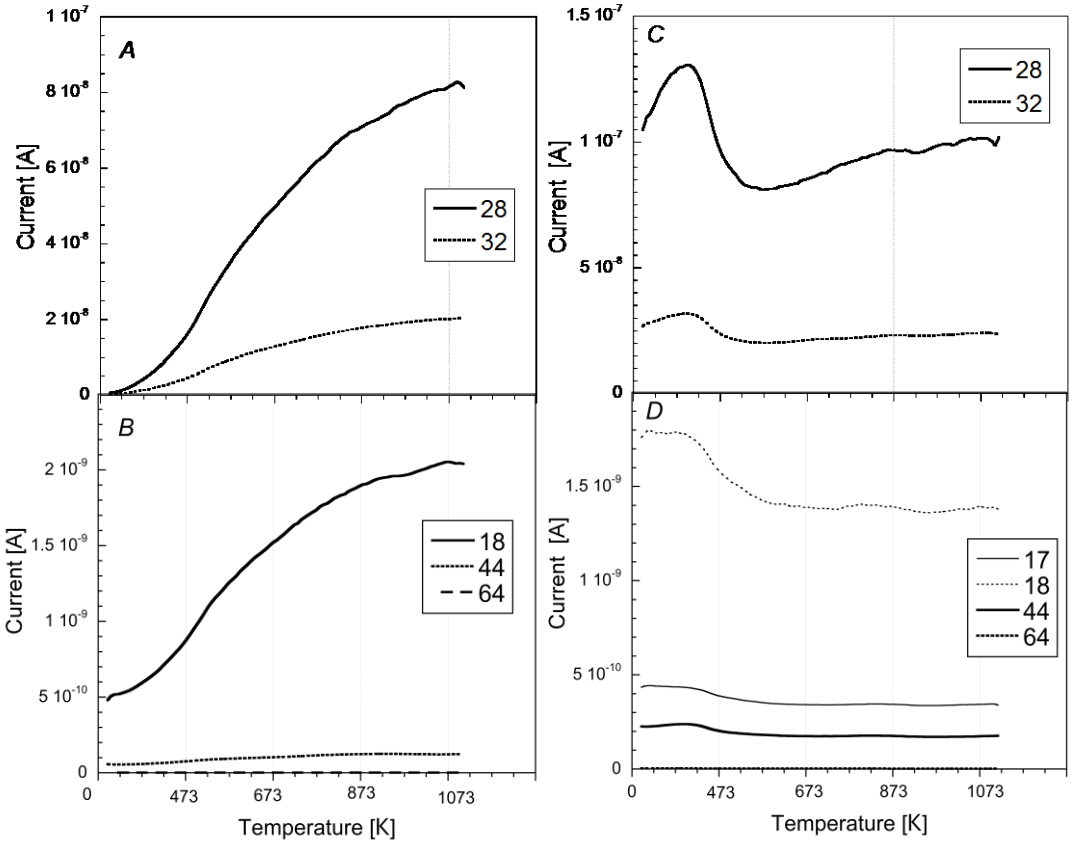

Figure 7. m/z (numbers presented in the legends) thermal profiles for HT-MPR (A and B) and HT-MRP (C and D). The profiles for m/z 64 are of low intensity and they overlap with the X-axis.

m/z thermal profiles for HT-MRP are different than those for HT-MPR (Figure 7), which support the hypothesis presented above on the effect of GO surface chemistry on the final properties of the monolith. For the former sample they show removal of oxygen (m/z 32) and decomposition of carboxylic groups (as water (m/z 17 and 18), CO (m/z 28), and CO_2 (m/z 44)) at low temperatures suggesting higher reactivity of the carbon phase [18]. On the other hand, on the surface of HT-MPR rather basic OH groups, quinones or carbonyls decompose at high

temperatures [18]. Those totally different thermal m/z patterns suggest that the different carbon phases are present in these two monoliths. They also differ from those for the carbon from the polymer (Figure 8S of Supplementary Information). The results support the hypothesis presented above that epoxy groups of GOM could react with sulfonic moieties of the polymer forming a specific resin/coating on the surface [16, 17]. Three-dimensional comparison of m/z profiles for the samples studied are collected in Figure 9S.

3.5 Porous properties

The analysis of the nitrogen adsorption isotherms (Figure 8 A) revealed that M, MR and HT-MR are the nonporous monoliths with the surface area not exceeding 3 m^2/g. On the other hand the carbon coated exhibits porous structure (Table 2). Interestingly, the carbon derived from the polymer itself does not exhibit any porosity which once again distinguishes it from the carbon described in Ref. [20] were a small surface area, 38 m^2/g, was reported. Apparently, carbonization conditions are an important factor determining the properties of the final products. Besides the surface area evaluated with the BET method, which is not accurate for very microporous materials [26], the surface area was also evaluated using SPE method [13]. Moreover the pore volume and surface area were obtained using NLDFT assuming the heterogeneous geometry of pores [14]. The BET surface area is smaller than the surface area from SPE and DFT methods, indicating that the pores are ultramicroporous [13]. Regardless the method, the HT-MPR is more porous than HT-MRP. Its surface area and volume of micropores are 21 and 17 % greater than those for the latter sample.

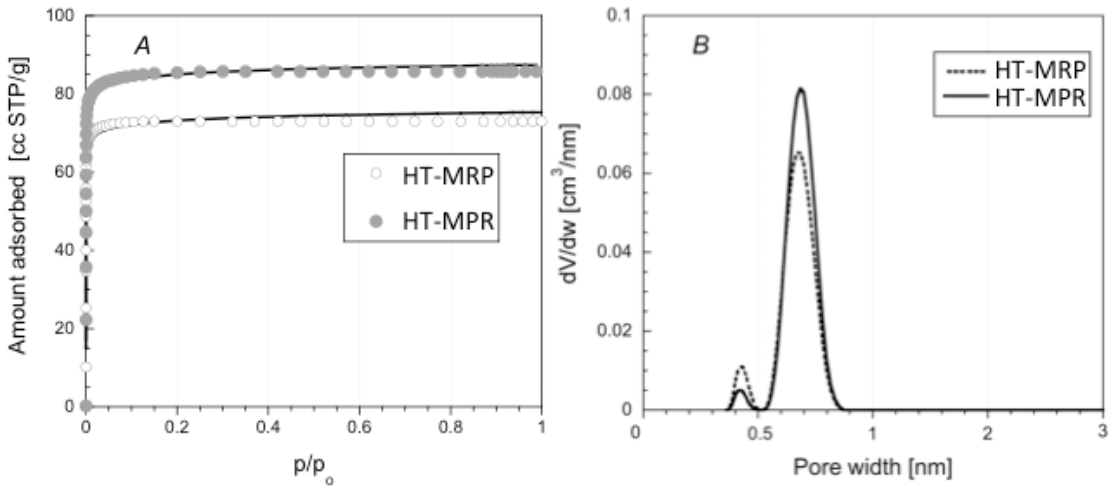

Figure 8. Nitrogen adsorption isotherms with the fit to NLDF (A) and pore size distributions (B) for the carbon reinforced graphene monoliths.

Table 2. The parameters of porous structure determined from the nitrogen adsorption isotherms.

Sample	S_{BET} [m^2/g]	S_{SPE} [m^2/g]	S_{DFT} [m^2/g]	$V_{< 1nm}=V_t$ [cm^3/g]	$V_{<0.5nm}$ [cm^3/g]
HT-MRP	229	345	328	0.107	0.007
HT-MPR	277	415	363	0.122	0.003

Slow kinetics of the adsorption isotherm measurements indicated the presence of ultramicropores. The pore size distribution from the NLDFT indicates evidently the presence of ultramicropores whose width is less than 0.7 nm in the both samples, as presented in Figure 7 B. Both monoliths can be considered as molecular sieves but HT-MPR is more homogeneous in the pore sizes. That 0.7 nm size of pores is identical for both samples implying the presence of an optimum interaction between the graphene sheets and newly introduced carbon. The higher volume of

pores in HT-MPR that that in HT-MRP is linked to the higher content of the porous carbon phase in the former monolith.

4. Conclusions

This paper shows the procedure leading to the production of relatively rigid graphene based monoliths having highly uniform ultramicroporosity. The process applied is environmentally friendly and uses a water soluble polymer with no washing of the final material required. The ultramicropores are uniformly developed in the monolith form, leading to efficient transport channels for molecules and ions. At the same time, the robust monolith has no interparticle gaps, offering high electrical conductivity. The developed monoliths have high application potentials for separation/molecular sieving and selective storage of gases and ions. The deposition of the porous phase on the conductive graphene based frames of an interconnected network with large void space will provide not only a fast electron transfer but also an easy access of the electrolytes to those pores where the most efficient electrical double layer charge storage is possible [24]. Another application, which requires the 0.7 nm pores of high volume, is a selective separation of CO_2 with the relevance to CO_2 sequestration [29, 30]. As this robust graphene monolith can be applied to a gas filter, we can sense small gas molecules on filtering using the electrical conductivity change for monitoring local environments.

Acknowledgement

The authors are grateful to Professor Morinobu Endo for supporting experimental studies. TJB expresses here gratitude to Drs. Toshihiko Fujimori, and Ryusuke Futumura for their patience and help with instrumental approaches and to Dr. Rodolfo Cruz-Silva for his experimental help for observation of SEM images.

This work was supported by Grant-in-Aid for Scientific Research (A) (24241-38) and Concert-Japan project: Efficient Energy Storage and Distributions, JST.

REFERENCES

1. Muhammad, Choong TSY, Chuah TG, Yunus R, Yap YHT. Adsorption of β-carotene onto mesoporous carbon coated monolith in isopropyl alcohol and n-hexane solution: equilibrium and thermodynamic study, Chem Eng J 2010; 164: 178-182
2. Silvestre-Albero A, Ramos-Fernández J M, Martínez-Escandell M, Sepúlveda-Escribano A, Silvestre-Albero J, Rodríguez-Reinoso F, High saturation capacity of activated carbons prepared from mesophase pitch in the removal of volatile organic compounds. Carbon 2010;48: 548-556.
3. Kubo T, Sakamoto H, Fujimori T, Itoh T, Ohba T, Kanoh H, Martinez-Escandell M, Ramos-Fernandez J M, Casco M, Rodriguez-Reinoso F, Urita K, Moriguchi I, Endo M, Kaneko K, Diffusion-barrier-free porous carbon monoliths as a new form of activated carbon. ChemSusChem 2012; 5:2271-2277.
4. Elaigwu SE, Greenway GM. Biomass derived mesoporous carbon monoliths via an evaporation-induced self-assembly. Mater Lett 2014;115:117–120.
5. Zhao X, Zhang Q, Chen CH-M, Zhang B, Reiche S, Wang A, Zhang T, Schlogl R. Su DS. Aromatic sulfide, sulfoxide, and sulfone mediated mesoporous carbon monolith for use in supercapacitor. Nano Energy 2012; 1: 624–630.
6. Wen P, Gao J, Zhang Y, Liu Y. Fabrication of chitosan scaffolds with tunable porous orientation structure for tissue engineering. J Biomater Sci, Polym Ed 2011;20:19–40.
7. Zhang N, Qiu H, Si Y, Wang W, Gao J. Fabrication of highly porous biodegradable monoliths strengthened by graphene oxide and their adsorption of metal ions. Carbon 2011;49 :827–37.
8. Wang S, Tristan F, Minami D, Fujimori T, Cruz-Silva R, Terrones M, Takeuchi K, Teshima K, Rodrıguez-Reinoso F, Endo M, Kaneko K. Activation routes for high

surface area graphene monoliths from graphene oxide colloids. Carbon 2014; 76: 220 –231.

9. Hummers, W. S.; Offeman, R. E., Preparation of Graphitic Oxide. J Am Chem Soc 1958, 80: 1339-1339.
10. Ogino I, Yokoyama Y, Iwamura S. Mukai SR Exfoliation of Graphite Oxide in Water without Sonication: Bridging Length Scales from Nanosheets to Macroscopic Materials. Chem Mater 2014;26:3334-3339.
11. Kaneko K, Jshi C, Ruike M, Kubawara H. Origin of superhigh surface area and microscystalline graphitic c structures of activated carbons. Carbon 1992; 30; 1075-1088.
12. Jagiello J, Olivier JP. Carbon slit pore model incorporating surface energetical heterogeneity and geometrical corrugation. Adsorption 2013; 19:777–783
13. .Huh SH. Thermal reduction of graphene oxide. In: Mikhailov S, editor. Physics and applications of graphene – experiments, InTech; 2011 p. 73-90.
14. Blank WJ. Isocyanate modified blocked sulfonic acid ester as a crosslinking catalyst. US patent EP0377931 B1 (1993).
15. McDonald MD. Metal coating compositions. US patent 2,885,312 (1959).
16. Figueiredo JL, Pereira MFR, Freitas MMA, Órfão JJM. Modification of the surface chemistry of activated carbons. Carbon 1999;37:1379-89.
17. Marsh H, Rodriguez-Reinoso F. Activated Carbon. Elsevier, Amsterdam. 2005.
18. Bandosz TJ, Castellon-Rodriguez E, Montenegro JM, Seredych M. Photoluminescence of nanoporous carbons: Opening a new application route for old materials Carbon 2014; 77: 651-659

19. Endo M, Maeda T, Takeda T, Kim YJ, Koshiba K, Hara H, Dresselhaus MS. Capacitance and pore-size distribution in aqueous and nonaqueous electrolytes using various activated carbon electrodes. J Electrochem Soc 2001;148:A910-4.
20. Liang J, Jiao Y, Jaroniec M, Qiao SZ. Sulfur and nitrogen dual-doped mesoporous graphene electrocatalyst for oxygen reduction with synergistically enhanced performance. Angew Chem Int Ed 2012;51:1-6; Angew Chem 2012;124:11664-8.
21. Xie G, Zhang K, Guo B, Liu Q, Fang L, Gong JR. Graphene-based materials for hydrogen generation from light-driven water splitting. Adv Mater 2013;25:3820-39.
22. Kudin, K. N.; Ozbas, B.; Schniepp, H. C.; Prud'homme, R. K.; Aksay, I. A.; Car, R., Raman Spectra of Graphite Oxide and Functionalized Graphene Sheets. Nano Letters 2007, 8 (1), 36-41.
23. Zawadzki J. IR spectroscopy in carbon surface chemistry. In: Thrower PA, editor. Chemistry and physics of carbon, vol 21, New York; Dekker; 1989 p. 180-200.
24. Gregg SJ, Sing KSW. Adsorption, Surface Area, & Porosity. Academic Press, New York, 1982.
25. Chmiola J, Yushin G, Gogotsi Y, Portet C, Simon P, Taberna P.L. Anomalous increase in carbon capacitance at pore sizes less than 1 nanometer. Science 2006;313:1760-1763.
26. Seredych M, Koscinski M, Sliwinska-Bartkowiak M, Bandosz TJ. Charge storage accessibility factor as a parameter determining the capacitive performance of nanoporous carbon-based supercapacitors. ACS Sustainable Chem Eng 2013;1:1024-1032.
27. Wickramarante NP, Jaroniec M. Importance of small micropores in CO_2 capture by

phenolic resin-based activated carbon spheres. J Mater Chem A 2013:1 : 112-116.

28. Seredych M, Jagiello J, Bandosz TJ. Complexity of on nanoporous CO_2 adsorption on sulfur-doped carbons – Is surface chemistry an important factor? Carbon 2014; 74:207-2017.

Captions to the Tables

Table 1.

Electrical resistance, estimated density and the ratios of the intensity of band representing defects to the band representing sp^2 configurations for the samples studied.

Table 2.

The parameters of porous structure determined from the nitrogen adsorption isotherms.

Captions to the Figures

Figure 1. Appearance of the monoliths, initial and after the final modifications. One grid on the background paper is 5 x 5 mm..

Figure 2. Comparison of the strength of the initial and modified monoliths. The diameter of HT-MRP monolith is 7 mm.

Figure 3. SEM images for MGO and HT-MR.

Figure 4. SEM images for the polymer treated monoliths

Figure 5. Figure 5. HRTEM images of the monolith texture.

Figure 6. Raman spectra for the series of the graphene-based (A) and carbon-reinforced monoliths (B).

Figure 7. m/z (numbers presented in the legends) thermal profiles for HT-MPR (A and B) and HT-MRP (C and D).

Figure 8. Nitrogen adsorption isotherms with the fit to NLDF (A) and pore size distributions (B) for the carbon reinforced graphene monoliths.